Available online at www.sciencedirect.com
ScienceDirect
Coordination Chemistry Reviews 251 (2007) 2674–2687
COORDINATION CHEMISTRY REVIEWS
www.elsevier.com/locate/ccr

Review

# Construction of redox- and photo-functional molecular systems on electrode surface for application to molecular devices

Hiroshi Nishihara *, Katsuhiko Kanaizuka, Yoshihiko Nishimori, Yoshinori Yamanoi

*Department of Chemistry, School of Science, The University of Tokyo, 7-3-1 Hongo, Bunkyo-ku, Tokyo 113-0033, Japan*

Received 27 December 2006; accepted 1 April 2007
Available online 5 April 2007

## Contents

1. Introduction ..... 2674
2. Redox-conducting metal complex oligomer wires prepared by stepwise coordination method on an electrode surface ..... 2675
   2.1. Bottom-up fabrication of the wires ..... 2675
   2.2. Electron transport behavior of the wires ..... 2679
3. Bio-photosensor composed of cyanobacterial photosystem I, molecular wire, gold nanoparticle, and transistor ..... 2683
4. Conclusion ..... 2686
   Acknowledgements ..... 2686
   References ..... 2686

**Abstract**

Two systems using bottom-up fabrication of molecular wires on an electrode surface are described. The first system involves films composed of linear and branched wires of metal complex oligomers, which were prepared using stepwise complexation of metal ions with bis- and tris-tpy (tpy = 2,2′:6′,2″-terpyridine) ligands, respectively, on tpy-terminated SAM on gold. This method allows the formation of desired numbers of polymer units and of desired sequences of hetero-metal structures in the polymer chain. The electron transport mechanism and kinetics for the redox reaction of the films of linear and branched oligomer wires analyzed by potential step chronoamperometry indicate that electron conduction occurs by successive electron hopping between neighboring redox sites within a molecular wire. The second system is an assembly of bio-conjugated materials to achieve the output of electrons directly from photosystem I (PSI) of thermophilic cyanobacteria to a gold nanoparticle on the gate of a field-effect transistor (FET) by bypassing the electron flow via a molecular wire. Photo-electrons generated by the irradiation of reconstituted PSI on the gate with 670–680 nm light were found to control the FET performance, which is sufficiently stable for use exceeding a period of 1 year.


*Keywords:* Bottom-up synthesis; Terpyridine; Photo-electron transfer; Electron transport; Redox conduction; Photosystem I; Photonsensing

## 1. Introduction

A variety of molecules with particular functionalities have been discovered and developed in recent years, and their assembly on solid surfaces for application to molecular devices has become an important research target [1–4]. Molecular devices are a key subject in nanotechnology, and can be roughly divided into two categories, dry and wet systems. Dry systems have been employed in semiconductor technology, dominating today's electronics, while wet systems have been realized in biomaterials, in which the highest performance has been achieved by the fine tuning of different molecular functionalities. Compared with dry systems, wet systems have a disadvantage in performance speed because of the slow mobility of ions, but they have an advantage in fine and precise control of the direction and kinetics of electron transfer even at room temperature, leading to a low noise level, because the electron transfer is governed by the absolute electrochemical potentials of a series of molecules coexisting in the system. Even a small potential difference in millivolt order can control the electron transfer definitely (5 mV is the noise level in a dry system at room temperature).

Control of the direction, kinetics, and efficiency of electron movement is an important and elementary issue for its application to molecular devices. As molecular wires assist in electron

* Corresponding author. Tel.: +81 3 5841 4346; fax: +81 3 5841 8063.
*E-mail address:* nisihara@chem.s.u-tokyo.ac.jp (H. Nishihara).

0010-8545/$ – see front matter © 2007 Elsevier B.V. All rights reserved.
doi:10.1016/j.ccr.2007.04.002

conduction, especially over a long range, plenty of recent interest has been focused on the electron transfer characteristics of molecular wires [5].

In the present article, we describe two different systems with which to construct electro- and photo-functional molecular assemblies on an electrode surface. The former is the bottom-up fabrication of redox-conducting metal complex polymers on an electrode surface and their redox conduction behavior [6–8]. The latter is the fabrication of a bio-photosensor by combining cyanobacterial photosystem I coupled with a transistor via a molecular wire [9]. These systems will be precursors of new types of molecular devices working in electrolyte solution.

## 2. Redox-conducting metal complex oligomer wires prepared by stepwise coordination method on an electrode surface

### 2.1. Bottom-up fabrication of the wires

Redox polymers, in which redox species are connected to form a polymer wire, are representative electron-conducting substances [10–14]. The invention of the redox polymer-coated electrode in the 1970s initiated both basic and applied research into electron transfer phenomena of redox polymer films [15]. Redox polymer films on an electrode surface, prepared mostly by polymer coating, chemical modification, and electrochemical polymerization, have been excellent substrates for experimental and theoretical studies on electron transport behavior [16–19]. In most of the previous studies, polymer chains were distributed randomly in the film (Fig. 1A), and thus the electron transport was treated according to the concept of "redox conduction," based on the diffusional motion of collective electron transfer pathways [20–23]. The apparent diffusion coefficient of collective electron transfer pathways in the film, $D_{app}$, composed of electron hopping terms and/or physical diffusion, is the key factor relating to the Dahms–Ruff equation [24,25] and the Laviron–Andrieux–Savéant theory [26].

Redox oligomer wires were fabricated recently on an electrode surface by the interfacial stepwise coordination method (Fig. 1B) [27–30], which is a flexible method for creating organic–inorganic assemblies through the incorporation of metal ions with desired properties and organic ligands [31–33]. Monolayer films with reactive terminal group have been extended into coordination polymers or supramolecular structures through covalent chemical reaction using layer-by-layer nanostructural growth [30,34–36]. If the building blocks were redox-active metal complexes, they would be of great interest in the investigation of fundamental aspects of charge transfer processes [27–29]. Based on the idea, we have fabricated homo- and hetero-metal complex oligomer and polymer wires of bis(terpyridine)metal complexes [6–8]. An important advantage of this method is that it affords organized structures of rigid redox polymer wires having the desired numbers of redox complex units perpendicular to the surface. It is also possible to prepare desired sequences of different metal complex units by changing the metal ion and bridging ligand sources in the stepwise coordination process. A typical method for fabricating multiple complex layers is as follows [6,8]. First, Au-S-AB-tpy SAM was prepared by immersing an Au/mica or Au/ITO plate in a chloroform solution of tpy-AB-SS-AB-tpy (Fig. 2). In the case of connecting the Fe(II) ion, the tpy-terminated surface was immersed in 0.1 M $Fe(BF_4)_2$ aq or $(NH_4)_2Fe(SO_4)_2$ aq, rinsed with water, and dried with a nitrogen blow. The bis(tpy)iron structure was prepared by immersing the film with a metal-terminated surface in a chloroform solution of an azobenzene-bridged bis-tpy ligand, $L_1$, followed by rinsing with chloroform and drying (Fig. 2B). The latter two processes were repeated for the preparation of multilayered (namely, polymeric) bis(tpy)iron(II) complex films.

In contrast, the mere combination of immersion in $CoCl_2$ aq and immersion in a chloroform solution of $L_1$ with the Au-S-AB-tpy SAM was not sufficient for accumulating bis(tpy)cobalt complex units [6]. We then added a process of electrochemical oxidation from Co(II) to Co(III) (that is, a combination of (a) immersion in $CoCl_2$ aq, (b) immersion in a chloroform solution of $L_1$, and (c) the holding of the plate at 0.3 V (versus $Ag/Ag^+$)). This successfully produced multilayered bis(tpy)cobalt complex films [6].

In this article, the film for the $n$th complexation cycles using metal ion and bridging ligand $L_x$ is abbreviated as [$n$M$L_x$]. The stepwise quantitative film formation was confirmed by UV–vis spectra and cyclic voltammetry (CV). For example, Fig. 3A shows the UV–vis spectrum of the bis(tpy)iron complex film, ($n$Fe$L_1$) ($n$ = 1–5), where absorbance of the peak at 592 nm ascribed to the MLCT transition increased almost linearly with the number of stepwise complexations, $n$ (Fig. 3B) [6]. In CV in Fig. 4A, $i_p$, which is the peak current of a reversible redox reaction of the $Fe^{III}/Fe^{II}$ couple appearing at 0.67 V versus ferrocenium/ferrocene ($Fc^+$/Fc) in $Bu_4NClO_4$–$CH_2Cl_2$, increases almost proportionally with $n$ (Fig. 4B), indicating a linear increase in the coverage of electroactive species.

The anodic charge integration under the voltammetric wave yields $\Gamma_{CV,[nFeL_1]} = 1.4 \times 10^{-10}$ mol cm$^{-2}$, approximately coincident with the maximum surface coverage based on the complex cation size (1.0 nm$^2$ per molecule). Another $p$-phenylene-bridged bis-tpy ligand, $L_2$, afforded similar results (Fig. 5A), showing perfect complexation on the terminal bridging ligands in every step, to give the surface coverage of $\Gamma_{CV,[nFeL_2]} = 1.0 \times 10^{-10}$ mol cm$^{-2}$ [8].

Branched molecular wires of metal complex oligomers can be prepared also by the stepwise coordination method (Fig. 2C) [8]. Branched oligomer wires of $Fe(tpy)_2$ were obtained using tpy-AB-SS-AB-tpy and a new three-way bridging ligand, 1,3,5-$C_6H_3(tpy)_3$, $L_3$. In this case, $\Gamma$ can be expected to increase with the number of complexation cycles, $n$, having the $2^n - 1$ relationship, if the coordination reaction at the terminals of the molecular wires is not perturbed by interwire or wire-to-gold surface steric repulsion. Fig. 5A shows cyclic voltammograms of [$n$Fe$L_3$] ($n$ = 1–4) in $Bu_4NClO_4$–$CH_2Cl_2$. The $\Gamma_{CV,[nFeL_3]}$ values, estimated from the amount of electricity in the anodic peak of the cyclic voltammogram, are shown in Fig. 5B, where an increase in $\Gamma$ obeying the $2^n - 1$ relationship occurred up to *ca.* $n$ = 4. This result is consistent with the molecular structures obtained by the MM+ calculation, which suggests that the interwire and wire-to-gold surface steric repulsion becomes sig-

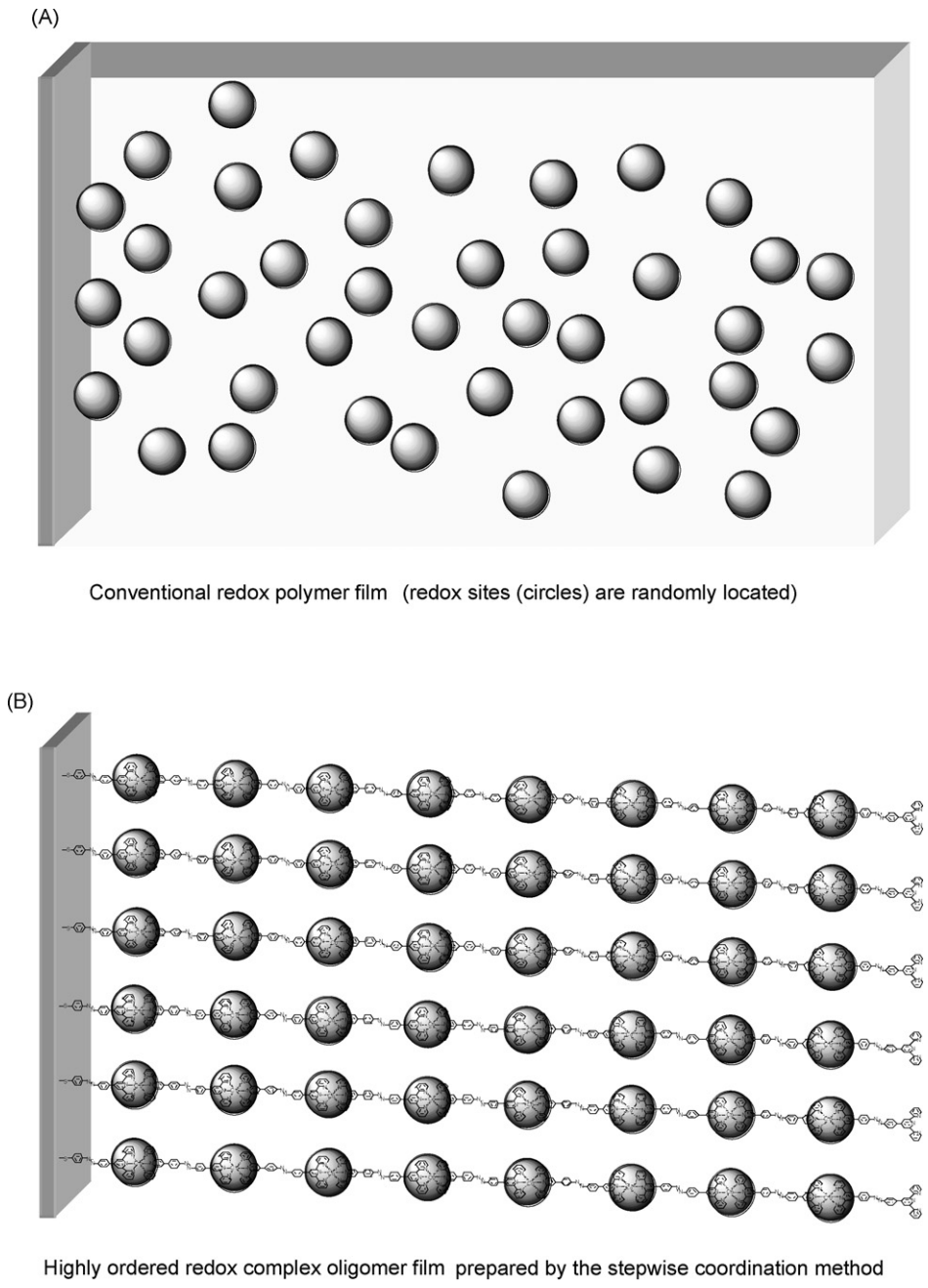


Fig. 1. Two types of redox polymer films on the electrode.

nificant at the fifth generation (Fig. 6). When $n$ was more than 4, the increase rate of $\Gamma$ slowed until it was similar to those of linear polymers, [$n$FeL$_2$], indicating that the wire can extend in only one dimension at higher generations.

The morphology of the complex oligomer wire films on the surface was investigated using scanning tunneling microscopy (STM) and scanning electron microscopy (SEM). The STM image of [2FeL$_1$] shows a nearly close packing of 6 nm-o.d. circular domains, indicating the stacking of molecular chains, and the formation of a fairly smooth surface, as shown in Fig. 7A [8]. The film of branched oligomers wires, [2FeL$_3$], shows a clearer image of domain structures that are evenly distributed in shape and size all over the surface (Fig. 7B). Fig. 7C and D shows STM images of the films with a combination of linear and branched oligomer wires, [1FeL$_2$$n$FeL$_3$] ($n$ = 3, 4), prepared in a short immersion time ($t_1$ = 10 s) of Au/mica in a chloroform solution of tpy-AB-SS-AB-tpy to make a sparse distribution of the oligomer wires [8]. The STM images showed circular dots whose diameters increased with the number of complexation cycles. These results strongly support the formation of ideal structures by the stepwise coordination method on the surface. The side view image of the SEM photograph for [47CoL$_1$] indicates the growth of the film to a thickness of *ca*. 100 nm (Fig. 8), which is reasonable as the value is near the product of the number of layers, 47 times the molecular unit length, 2 nm [6].

One merit of the stepwise coordination method is to allow creation of hetero-metal polymer chains with an intended sequence [15–19]. The stepwise formation of a hetero-metal double-layer

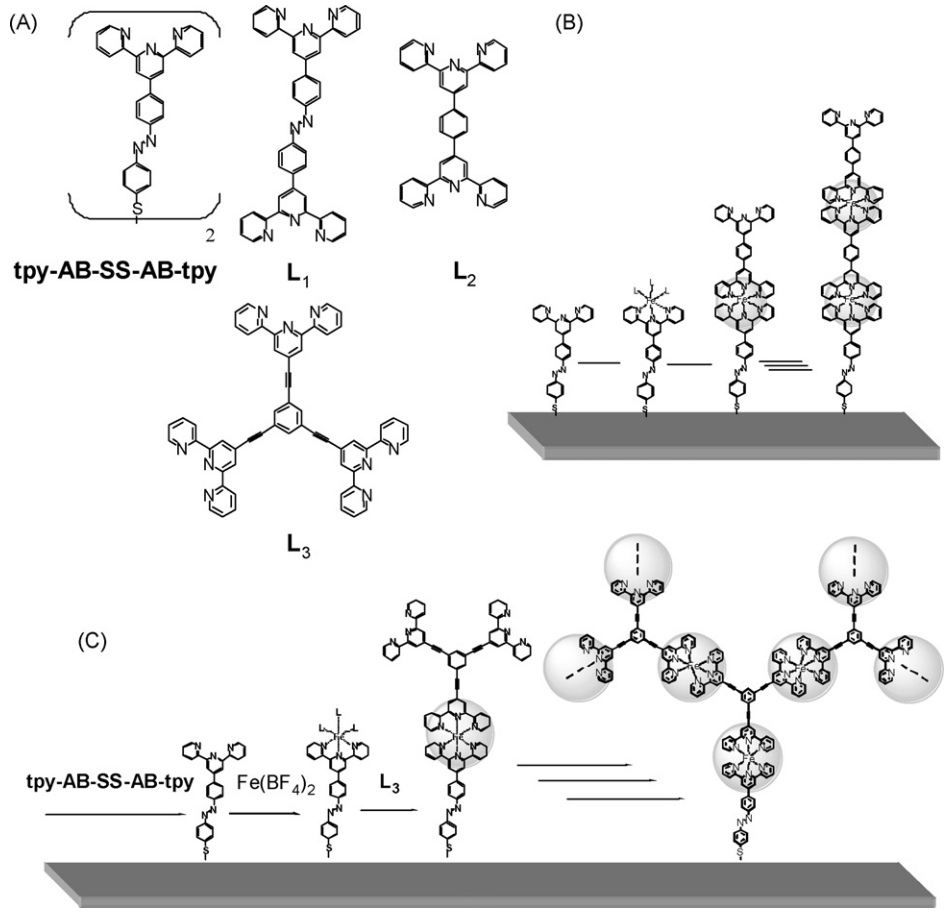


Fig. 2. Stepwise coordination methods to prepare linear and branched oligomer wires.

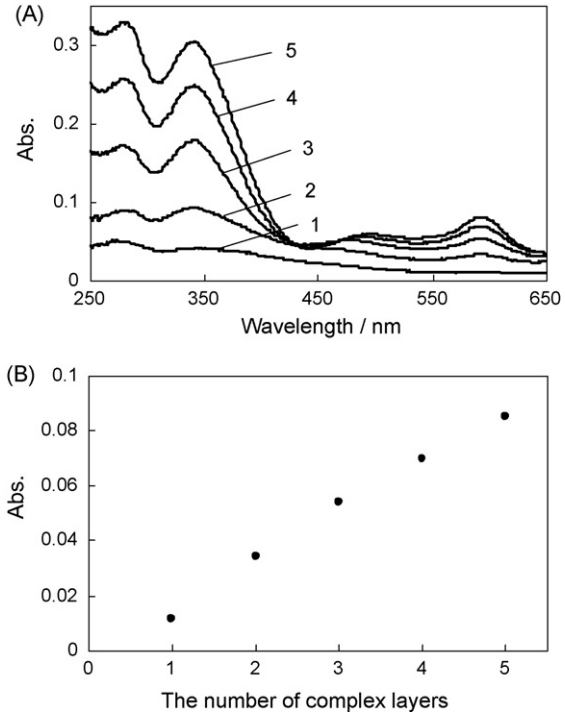


Fig. 3. Absorption spectra of [$n$FeL$_1$] ($n$ = 1–5) (A) and plots of the absorption peak (592 nm) vs. the number of complex layers (B).

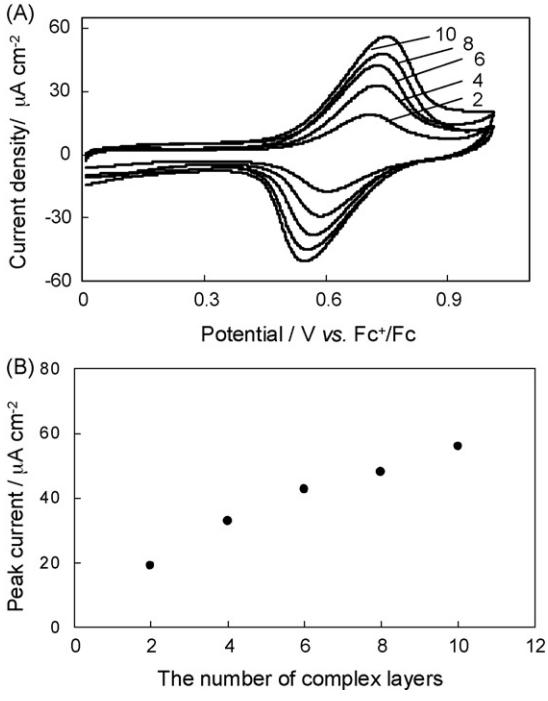


Fig. 4. Cyclic voltammograms of [$n$FeL$_1$] ($n$ = 2, 4, 6, 8, and 10) in 0.1 M $Bu_4NClO_4$–$CH_2Cl_2$ at a scan rate of 0.1 V s$^{-1}$ (A), and plots of the anodic peak current ($j_{pa}$) vs. the number of complex layers (B).

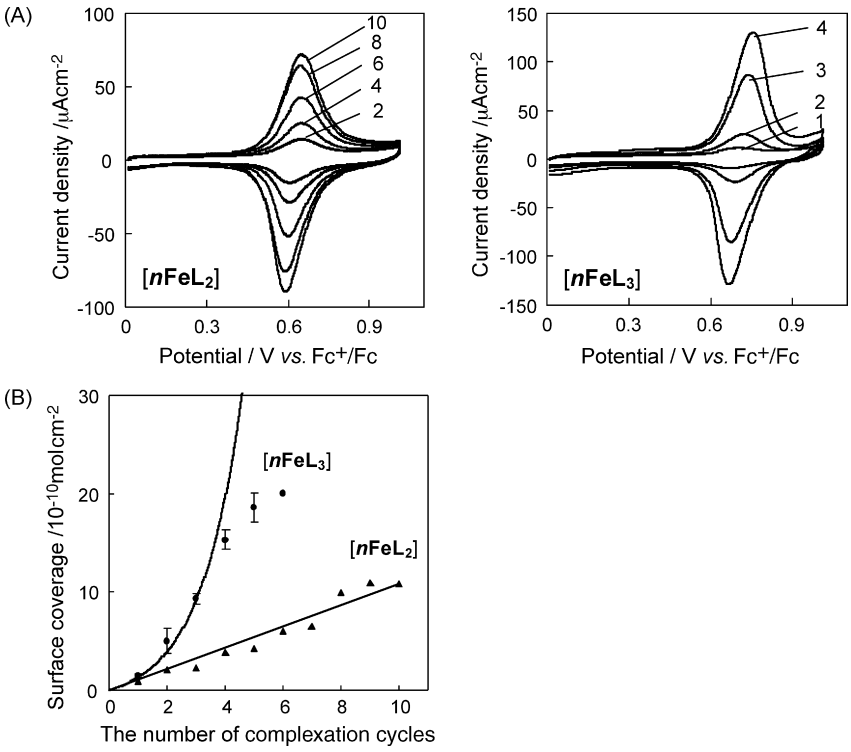


Fig. 5. Cyclic voltammograms of [$n$FeL$_2$] ($n$ = 2, 4, 6, 8, 10) and [$n$FeL$_3$] ($n$ = 1–4) in 1 M $Bu_4NClO_4$–$CH_2Cl_2$ at a scan rate of 0.1 V s$^{-1}$ (A), and plots of the coverage of redox-active sites, $\Gamma$ (mol cm$^{-2}$) vs. $n$ for [nFeL$_2$] and [$n$FeL$_3$] (B). The lines in the figure denote the relationship of $\Gamma = C \times n$ for [$n$FeL$_2$] and that of $\Gamma = C\,(2^n - 1)$ for [$n$FeL$_3$].

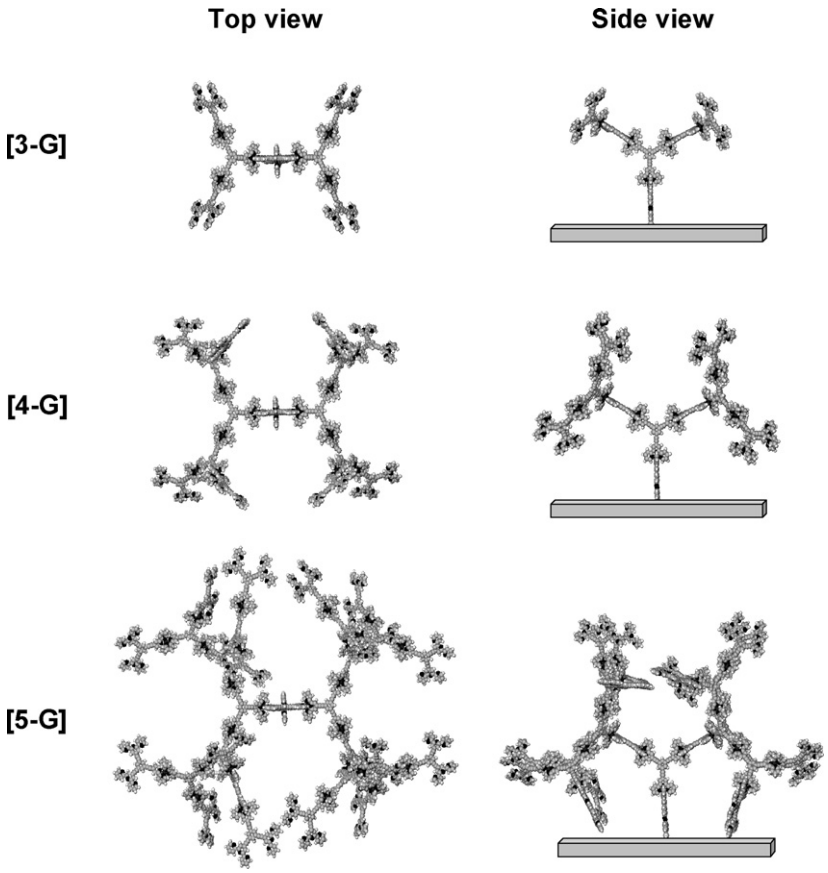


Fig. 6. Molecular structures of [$n$FeL$_3$] ($n$ = 3, 4, 5) obtained by MM+ calculation.

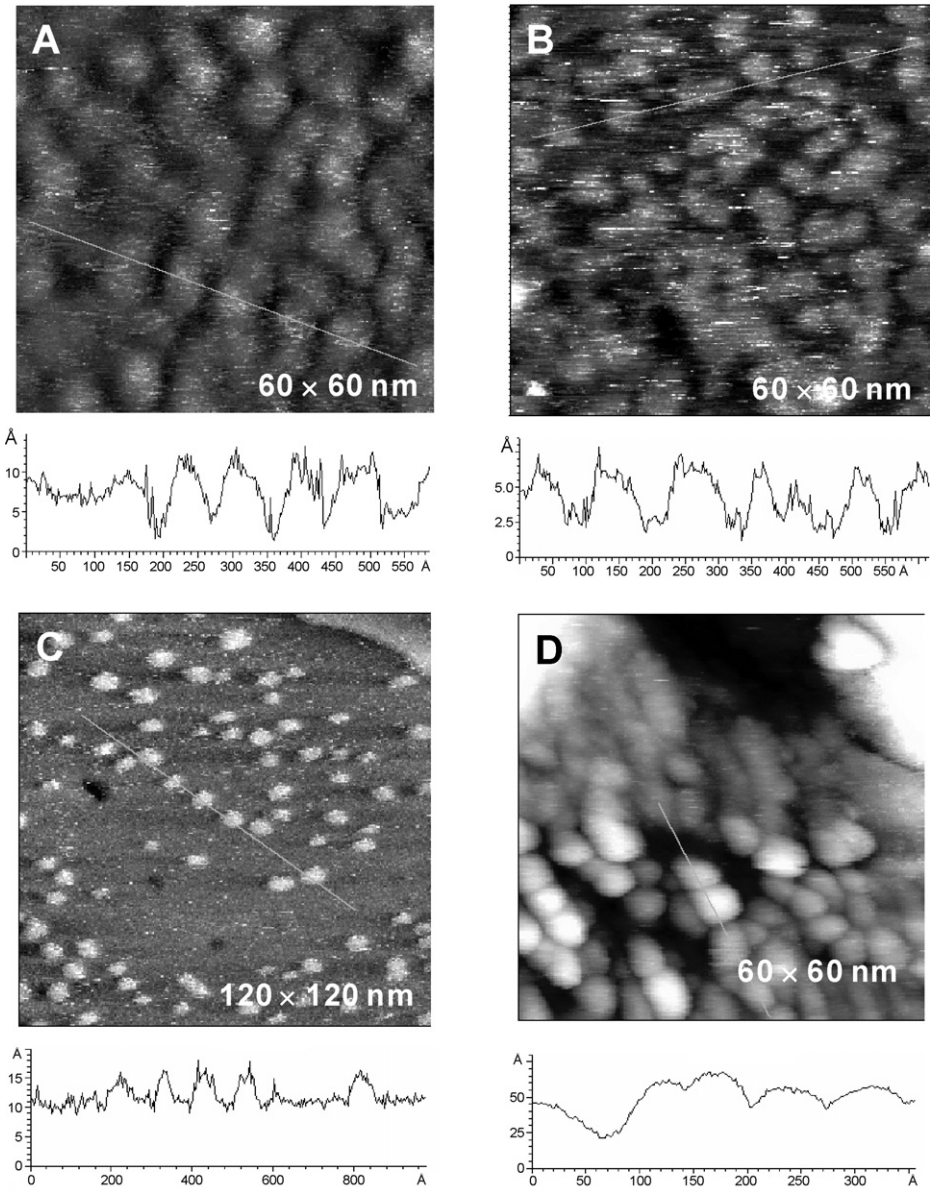


Fig. 7. STM images of [2FeL$_1$] (A), [2FeL$_3$] (B), and [1FeL$_2$*n*FeL$_3$] ($n = 3$, 4, $t_1 = 10$ s) (C and D).

film [1CoL$_1$1FeL$_1$] was monitored by CV during film construction (Fig. 9A), where the redox activity of the $Fe^{III}/Fe^{II}$ couple appeared without changing the redox activity of the $Co^{III}/Co^{II}$ couple when the bis(tpy)iron complex units were connected to the initially prepared bis(tpy)cobalt complex layer. In the CV of hetero-structured polymer films made of polymer chains composed of [10CoL$_1$5FeL$_1$] (Fig. 9B), the peak current for $Co^{II}/Co^{I}$ was larger than that for $Co^{III}/Co^{II}$ due to the difference in electron self-exchange rate constant values [37]. Also, the redox wave of $Fe^{III}/Fe^{II}$ was less than two-thirds the size of the $Co^{II}/Co^{I}$ redox wave due to the existence of a cobalt complex sequence between the electrodes, which acts as a barrier to electron transfer of the Fe complex even though $Fe^{III}/Fe^{II}$ is a fast electron-exchange couple. However, the retardation is very small, given that the barrier layer is thick (21 nm), suggesting the high electron transport ability of the inner π-conjugated Co(tpy)$_2$ polymer chain. A Co–Ru hetero-metal complex wire, [1CoL$_4$1Ru], was fabricated by stepwise coordination reactions at the gold surface using a ruthenium complex-attached terpyridine ligand, L$_4$, and it underwent reversible redox reactions of both redox complex units (Fig. 10) [7].

### 2.2. Electron transport behavior of the wires

If the redox conduction occurs in a diffusional motion and if the diffusion process within the redox polymer film on the electrode is the rate-determining step (i.e., if the electron transfer kinetics between the electrode and the nearest redox sites in the film are sufficiently fast), the current–time curve after the potential step that causes the redox reaction of the redox polymer film obeys the Cottrell equation,

$$i = -n_e FAD_{app}^{1/2} \frac{C}{(\pi t)^{1/2}} \quad (1)$$

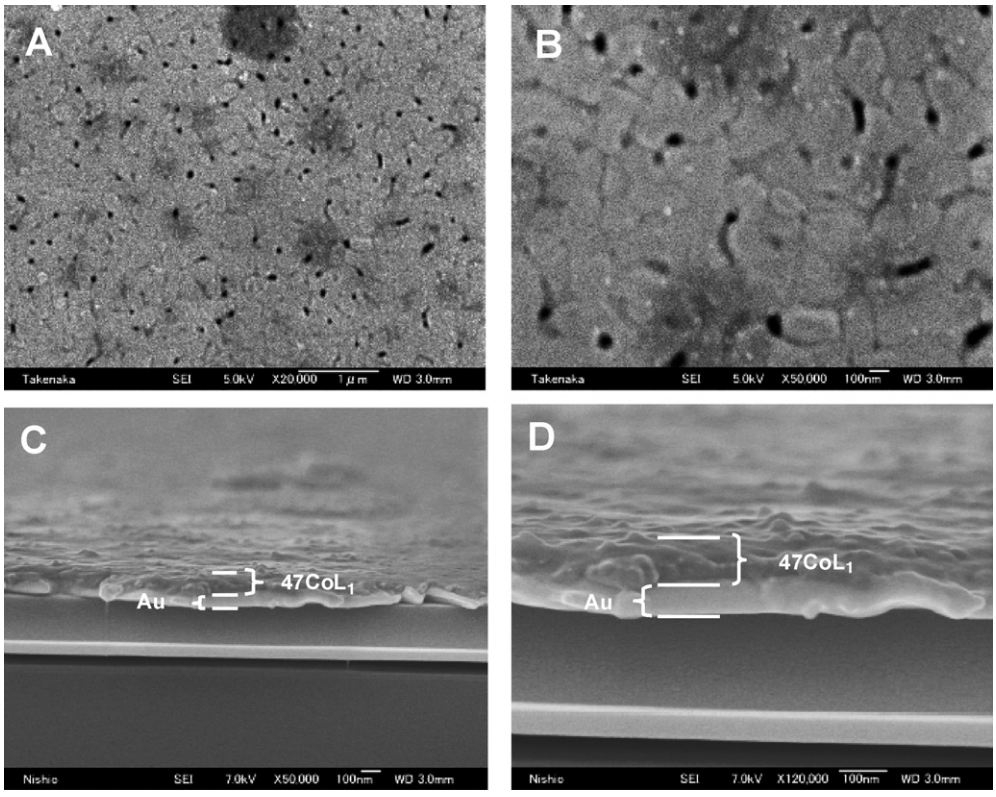


Fig. 8. SEM images of [47CoL$_1$].

where $n_e$, $F$, $A$, and $C$ refer to the number of electrons, the Faraday constant, the electrode area, and the concentration of redox sites in the film, respectively, and the current versus time ($i$–$t^{1/2}$) plot shows a linear line, until the diffusion layer reaches the film surface on the solution side [38–48]. The migration effect and counterion motion are also important in $D_{app}$ [49–52]. Potential step chronoamperometry (PSCA) is a simple method for evaluating $D_{app}$ [53].

PSCA was used to investigate the electron transport behavior of the Fe(tpy)$_2$ oligomer wires prepared by the stepwise coordination method on a gold electrode. Fig. 11 displays the $i$–$t$ plots after the potential step from 0.96 to 0.36 V versus Fc$^+$/Fc to reduce the Fe$^{II}$ complex moieties in linear Fe(tpy)$_2$ oligomer wires, [$n$FeL$_2$] ($n$ = 2, 4, 6, and 8) and in branched oligomer wires [$n$FeL$_3$] ($n$ = 2, 3, and 4), in 1 M Bu$_4$NClO$_4$–CH$_2$Cl$_2$. In all cases, the curvatures for the Fe$^{III}$/Fe$^{II}$ couple showed a quasi-plateau region in the initial period, followed by a rapid decrease in current. These features cannot be explained by the diffusion-limited redox conduction [38–48]. Compared to the PSCA behavior of the linear wires [$n$FeL$_2$] (*ca.* 0.05 s for [8FeL$_2$]; see Fig. 11A), the branched wires [$n$FeL$_3$] showed much longer time constant current flow behavior (*ca.* 0.1 s for [4FeL$_3$], see Fig. 11B). This difference strongly indicates the dominance of the through-bond electron transport pathway, because the density of redox sites in the branched oligomer film is expected to be similar to or higher than that of the linear oligomer films; thus,

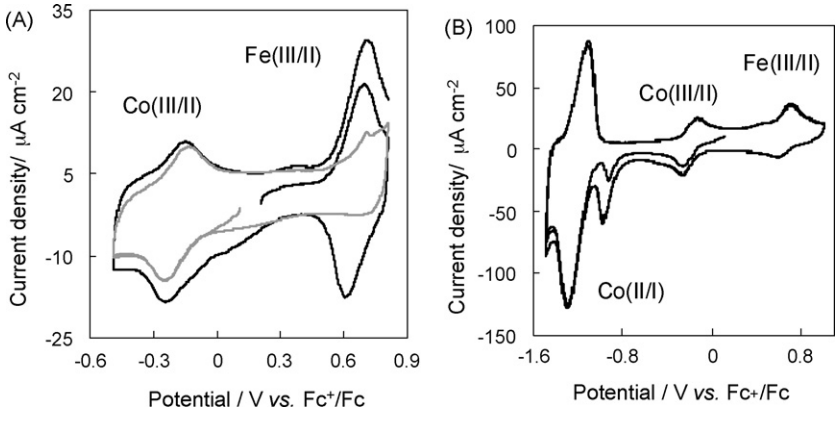


Fig. 9. Cyclic voltammograms of [1CoL$_1$] (gray) and [1CoL$_1$1FeL$_1$] (black) (A) and [10CoL$_1$5FeL$_1$] (B) on gold at 0.1 V s$^{-1}$ (reprinted with permission from Ref. [6]).

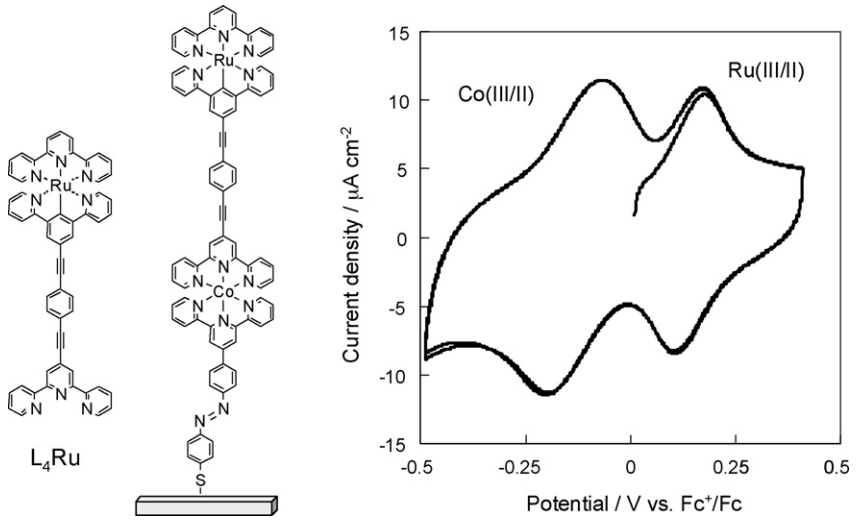


Fig. 10. A cyclic voltammogram of [1CoL$_4$1Ru] film on Au at a scan rate of 0.1 V s$^{-1}$ in 0.1 M $Bu_4NClO_4$–$CH_2Cl_2$.

the simple diffusion process containing through-space electron transfer of the former would give similar or faster electron transport kinetics than the latter.

The uncommon *i–t* characteristics for both linear and branched polymer wires could be explained by the electron transfer mechanism in a single molecular wire based on the molecular-level sequential chemical reaction, as displayed in Fig. 12. The concept of the mechanism is as follows. When the oxidized form in the film of molecular wires, Ox's, is reduced to Red and the back electron transfer can be neglected by applying a sufficient overpotential in PSCA, the electron transfer kinetics in the case of the *n*th complex sequence can be written as follows:

$$\begin{aligned}
&\mathrm{Ox}_1 + \mathrm{e}^- \rightarrow \mathrm{Red}_1, && \text{rate constant : } k_1 \quad \text{(a)}\\
&\mathrm{Red}_1 + \mathrm{Ox}_2 \rightarrow \mathrm{Ox}_1 + \mathrm{Red}_2, && \text{rate constant : } k_2 \quad \text{(b)}\\
&\mathrm{Red}_2 + \mathrm{Ox}_3 \rightarrow \mathrm{Ox}_2 + \mathrm{Red}_3, && \text{rate constant : } k_3 \quad \text{(c)}\\
&\vdots\\
&\mathrm{Red}_{n-1} + \mathrm{Ox}_n \rightarrow \mathrm{Ox}_{n-1} + \mathrm{Red}_n, && \text{rate constant : } k_n \quad \text{(d)}
\end{aligned} \tag{2}$$

where $\mathrm{Red}_i$ and $\mathrm{Ox}_i$ are reduced and oxidized forms, respectively, in the *i*th layer or generation in the film, and

$$\begin{aligned}
&\frac{\mathrm{d}[\mathrm{Ox}_1]}{\mathrm{d}t} = -k_1[\mathrm{Ox}_1] + k_2([\mathrm{Ox}_1]_0 - [\mathrm{Ox}_1])[\mathrm{Ox}_2] && \text{(a)}\\
&\frac{\mathrm{d}[\mathrm{Ox}_2]}{\mathrm{d}t} = -k_2([\mathrm{Ox}_1]_0 - [\mathrm{Ox}_1])[\mathrm{Ox}_2] + \frac{[\mathrm{Ox}_3]_0}{[\mathrm{Ox}_2]_0}k_2([\mathrm{Ox}_2]_0 - [\mathrm{Ox}_2])[\mathrm{Ox}_3] && \text{(b)}\\
&\frac{\mathrm{d}[\mathrm{Ox}_3]}{\mathrm{d}t} = -\frac{[\mathrm{Ox}_3]_0}{[\mathrm{Ox}_2]_0}k_2([\mathrm{Ox}_2]_0 - [\mathrm{Ox}_2])[\mathrm{Ox}_3] + \frac{[\mathrm{Ox}_4]_0}{[\mathrm{Ox}_2]_0}k_2([\mathrm{Ox}_3]_0 - [\mathrm{Ox}_3])[\mathrm{Ox}_4] && \text{(c)}\\
&\vdots\\
&\frac{\mathrm{d}[\mathrm{Ox}_{n-1}]}{\mathrm{d}t} = -\frac{[\mathrm{Ox}_{n-1}]_0}{[\mathrm{Ox}_{n-2}]_0}k_2([\mathrm{O}_{n-2}]_0 - [\mathrm{Ox}_{n-2}])[\mathrm{Ox}_{n-1}] + \frac{[\mathrm{Ox}_n]_0}{[\mathrm{Ox}_{n-2}]_0}k_2([\mathrm{Ox}_{n-1}]_0 - [\mathrm{Ox}_{n-1}])[\mathrm{Ox}_n] && \text{(d)}\\
&\frac{\mathrm{d}[\mathrm{Ox}_n]}{\mathrm{d}t} = -\frac{[\mathrm{Ox}_n]_0}{[\mathrm{Ox}_{n-2}]_0}k_2([\mathrm{Ox}_{n-1}]_0 - [\mathrm{Ox}_{n-1}])[\mathrm{Ox}_n] && \text{(e)}
\end{aligned} \tag{3}$$

where $[\mathrm{Ox_i}]_0$ and $[\mathrm{Ox_i}]$ are the initial and present two-dimensional concentrations, respectively, of the oxidized form of the redox moiety in the *i*th layer or generation in mol cm$^{-2}$. The reaction kinetics are controlled by two factors: $k_1$ (s$^{-1}$), for the electron transfer between the nearest redox site and the electrode (the electron transfer model for four complex layers is described), and $k_2$ (cm$^2$ mol$^{-1}$ s$^{-1}$), for the electron transfer between the neighboring redox sites in a molecular wire (in a primary approximation, the neighboring-site electron transfer rate constant in a polymer wire can be constant). In the case of linear oligomer wires, [*n*FeL$_1$] and [*n*FeL$_2$],

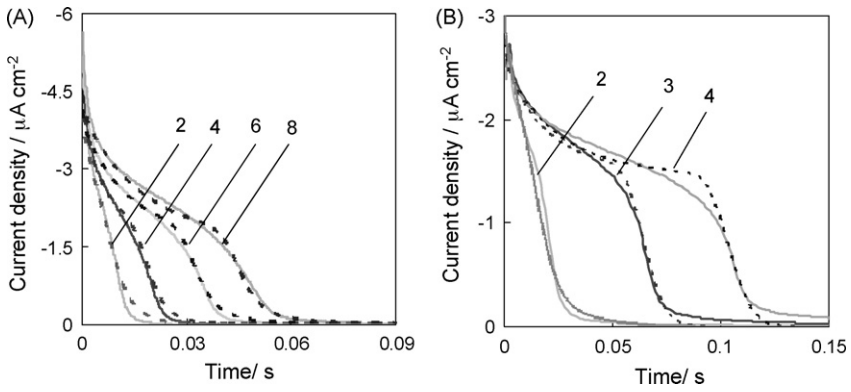


Fig. 11. The *i–t* plots after the potential step from 0.96 to 0.36 V vs. $Fc^+/Fc$ to reduce the $Fe^{III}$ complex moieties in [$n$FeL$_2$] ($n$ = 2, 4, 6, and 8) (A) and in [$n$FeL$_3$] ($n$ = 2, 3, and 4) (B) in 1 M $Bu_4NClO_4$–$CH_2Cl_2$ (solid lines). The numbers in the figure refer to $n$. Simulated curves in dotted lines are obtained with $k_1 = 240\,s^{-1}$, $k_2(L_2) = 1.7 \times 10^{13}\,cm^2\,mol^{-1}\,s^{-1}$, and $C_{dl} = 10\,\mu C\,cm^{-2}$ for [2FeL$_2$]; $k_1 = 240\,s^{-1}$, $k_2(L_2) = 1.7 \times 10^{13}\,cm^2\,mol^{-1}\,s^{-1}$, and $C_{dl} = 12\,\mu C\,cm^{-2}$ for [4FeL$_2$]; $k_1 = 210\,s^{-1}$, $k_2(L_2) = 1.6 \times 10^{13}\,cm^2\,mol^{-1}\,s^{-1}$, and $C_{dl} = 27\,\mu C\,cm^{-2}$ for [6FeL$_2$]; and $k_1 = 210\,s^{-1}$, $k_2(L_2) = 1.2 \times 10^{13}\,cm^2\,mol^{-1}\,s^{-1}$ and $C_{dl} = 40\,\mu C\,cm^{-2}$ for [8FeL$_2$] for A, and obtained with $k_1 = 270\,s^{-1}$, $k_2(L_2) = 4.9 \times 10^{13}\,cm^2\,mol^{-1}\,s^{-1}$ and $C_{dl} = 19\,\mu C\,cm^{-2}$ for [2FeL$_3$]; $k_1 = 270\,s^{-1}$, $k_2(L_3) = 5.0 \times 10^{12}\,cm^2\,mol^{-1}\,s^{-1}$, and $C_{dl} = 19\,\mu C\,cm^{-2}$ for [3FeL$_3$]; and $k_1 = 260\,s^{-1}$, $k_2(L_3) = 4.4 \times 10^{12}\,cm^2\,mol^{-1}\,s^{-1}$, and $C_{dl} = 27\,\mu C\,cm^{-2}$ for [4FeL$_3$].

$$[Red_1] + [Ox_1] = [Red_2] + [Ox_2] = [Red_3] + [Ox_3] = \cdots = [Red_n] + [Ox_n] = \text{constant} \quad (4)$$

and in the case of branched oligomer wires, [$n$FeL$_3$],

$$[Ox_1] + [Red_1] = \frac{[Ox_2] + [Red_2]}{3} = \frac{[Ox_3] + [Red_3]}{7} = \cdots = \frac{[Red_n] + [Ox_n]}{2^n - 1} = \text{constant} \quad (5)$$

The actual current can be observed as d[$Ox_1$]/d$t$. If the electron transfer between the neighboring redox sites is faster than that between the nearest redox site and the electrode, the reaction kinetics can be regarded as a "zero-order reaction," which implies that the constant current flows in the initial period. The simulation carried out in a numerical calculation that takes into consideration the double-layer capacitance, which decays exponentially with time, indicated that the simulated curves with parameters $k_1 = 220 \pm 10\,s^{-1}$ and $k_2(L_2) = 1.4 \pm 0.1 \times 10^{13}\,cm^2\,mol^{-1}\,s^{-1}$

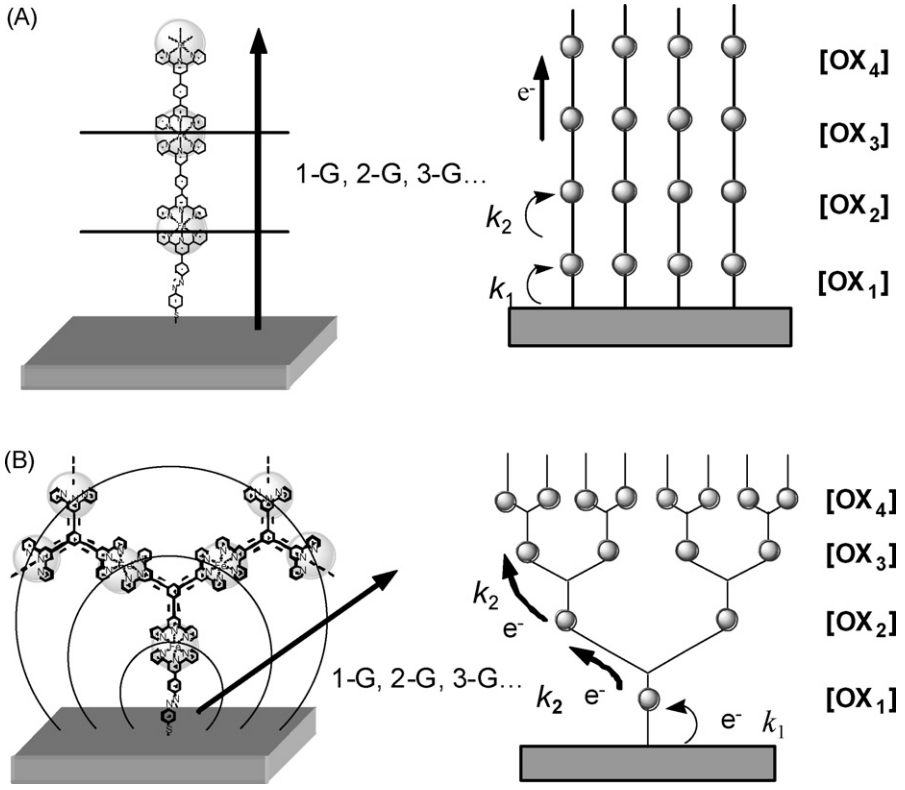


Fig. 12. Schematic illustration of the electron transfer mechanism in linear and branched molecular wires for A and B, respectively.

and $C_{dl} = 25 \pm 15\ \mu C\ cm^{-2}$ reproduce fairly well all of the experimental results of [$n$FeL$_2$] ($n$ = 2, 4, 6, and 8), as shown in Fig. 11A. The $i$–$t$ curvature for the film of [$n$FeL$_3$] ($n$ = 2, 3, and 4) could also be simulated using parameters $k_1 = 260 \pm 10\ s^{-1}$ and $k_2(L_3) = 4.8 \pm 0.2 \times 10^{12}\ cm^2\ mol^{-1}\ s^{-1}$ with the inclusion of $C_{dl}$ of $22 \pm 4\ \mu C\ cm^{-2}$ (Fig. 11B). The similarity of the $k_1$ values between [$n$FeL$_2$] and [$n$FeL$_3$] is logical because the first Fe layer is the same in both cases. The $k_2$ value for the branched oligomer wire is lower than that for the linear wire because the bridging ligand is *m*-phenylene in the former and *p*-phenylene in the latter and thus the former has a shorter π-conjugation.

The effects of electrolyte concentration on the kinetics were also analyzed. All the $i$–$t$ characteristics with different $n$'s at a given electrolyte concentration could be simulated using similar $k_1$ and $k_2$ values, but the strong dependence of $k_1$ and $k_2$ on the electrolyte concentration is reasonable because it is known that electron hopping is limited by the counterion motion [49–53]. The $k_1$ and $k_2$ values became almost constant at electrolyte concentrations above 1 M. This can be explained by the fact that the concentration of redox sites in the film is an estimated 1 M, and thus the limitation by counterion motion becomes small at high counterion concentration.

In conclusion, the quantitative formation of homo- and hetero-structured films at the surface was achieved by selecting the conditions of stepwise complexation reactions. This surface bottom-up method gave three-dimensional molecular wire assemblies in which through-bond electron transport is dominant. This methodology will lead to a new strategy for the molecular design of electronically functional molecular wires suitable for the development of molecular electronic devices.

## 3. Bio-photosensor composed of cyanobacterial photosystem I, molecular wire, gold nanoparticle, and transistor

Recently, opportunities for applying nanotechnology to biotechnology have developed, because many nanotechnology and biological systems operate in the same size scale [54–57]. Electronic communication of biomaterials with electronic transducers is a fundamental challenge in the rapidly developing field of bioelectronics.

Willner and his co-workers reported that the electrical communication of glucose oxidase (GOx) was accomplished by the reconstitution of the apo-GOx on a flavin adenine dinucleotide (FAD) functionalized gold nanoparticle (diameter: 1.4 nm) which was linked to the gold electrode surface by the 1,4-benzenedithiol monolayer (Fig. 13) [58,59]. This study indicated that unprecedented effective electron transfer from the FAD moiety to the electrode occurred through the Au-NP (electron transfer turnover rate $4500\ s^{-1}$). In a control experiment, a gold electrode modified with an FAD monolayer on which apo-glucose oxidase was reconstituted lacked electrical communication with the electrode. This unprecedented efficient electron transfer communication between redox protein and the electrode originated from the mediated electron transfer by a single gold nanoparticle that is conjugated to the protein assembly. This effective electron transfer communication between the nanoengineered redox enzyme and the electrode has important consequences on the sensitivity and selectivity of the enzyme electrode.

Photosynthesis is one of the most efficient processes in nature, in which almost 100% efficient photo-electric conversion systems are involved in the primary process [60,61]. High performance of photosystem I (PSI) is the result of its well-designed spatial configuration (position, direction, etc.). A large number of trials have been conducted to date involving the application of such biological systems to electronic devices. For example, chloroplasts were coated on an $SnO_2$ electrode and were examined as photoelectrochemical cells [62–66]. However, few investigations have used a PSI photonic device based on molecular-level assembly. Recently, we succeeded in the direct coupling between functional bionic components, PSI and an artificial electronic device (a field-effect transistor (FET)) via a molecular wire designed at the molecular-level (Fig. 14).

The PSI of *Thermosynechococcus elongatus* BP-1 was employed as a component of the bio-photosensor because of its high thermal stability at temperatures above 55 °C [67] and the efficient electron transfer activity of the isolated PSI [68–70]. The PSI is composed of 12 protein subunits possessing a well-ordered electron transfer chain. The molecular structure of PSI,

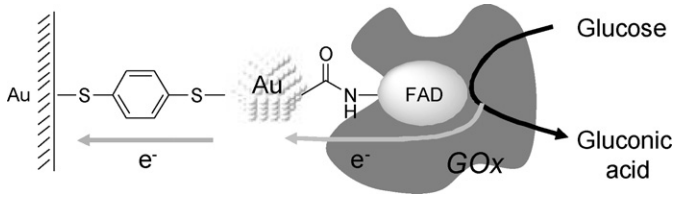


Fig. 13. Electron transfer process of nanostructured "enzyme (GOx)-gold nanoparticle-gold electrode surface".

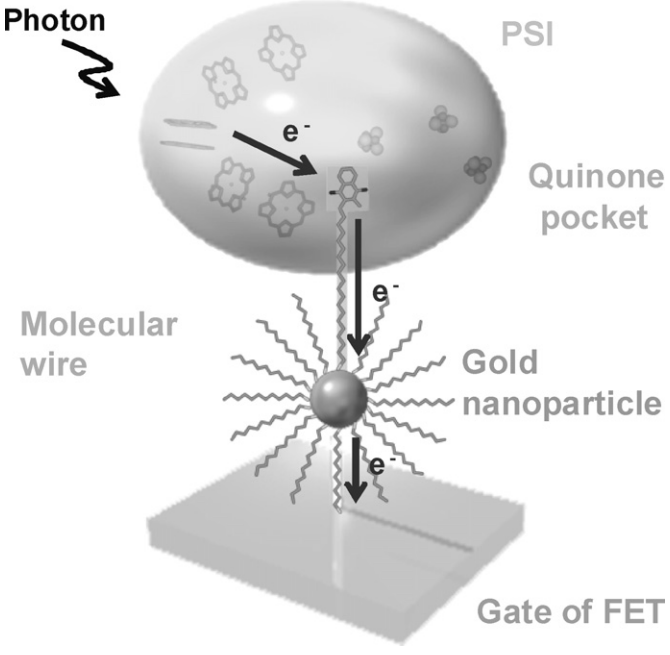


Fig. 14. The concept of the bio-photosensor made of PSI coupled with a transistor via molecular wire (reprinted with permission from Ref. [9]).

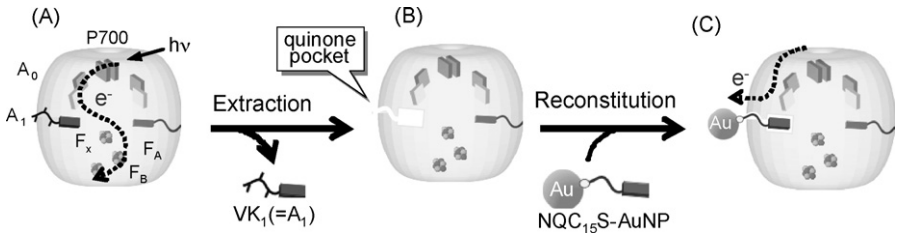


Fig. 15. Schematic illustration of the procedure for the reconstitution of PSI with a molecular wire: (A) intact PSI, (B) $VK_1$-free PSI, and (C) $NQC_{15}S$-AuNP@PSI (reprinted with permission from Ref. [9]).

the electron transfer mechanism and kinetics in PSI, and the treatment of living materials for the extraction of PSI have previously been investigated [71–76]. When PSI is irradiated, P700 is excited, and then a step-wise electron transfer from P700 to $F_B$ via $A_0$, $A_1$ (vitamin $K_1$; $VK_1$), $F_x$, and $F_A$ occurs without any backward transfer. These events induce a through-membrane charge separation, and the resulting efficiency of electron transfer is approximately 100% [60,61].

A schematic illustration of the procedure for the reconstitution of PSI with a molecular wire is shown in Fig. 15. Initially, $VK_1$ was extracted from the isolated intact PSI (Fig. 15A and B) using 50% water-saturated diethyl ether. Second, the $VK_1$-free PSI was reconstituted with a specifically designed molecular wire, $NQC_{15}S$-AuNP (1-[15-(3-methyl-1,4-naphthoquinon-2-yl)]pentadecyl thiolate protected gold nanoparticle), which possesses three advantageous characteristics: (1) a naphthoquinone unit located at the end of a molecular wire to fit into the pocket where $VK_1$ has been extracted, (2) a redox potential of naphthoquinone suitable for the output of electrons from the $A_0$ site to a molecular wire, and (3) a sufficient molecular length of the wire for the output of electrons from the pocket lacking $VK_1$ to the surface external to PSI. An alkyl chain was used as the molecular wire because the alkyl chain assists long range transfer more effectively than space [5]. The naphthoquinone-sulfur-linked molecular wire equipped with a gold nanoparticle ($NQC_{15}S$-AuNP, particle size: *ca.* 1.6 nm) [77] was treated with $VK_1$-free PSI in an MES buffer solution under cool and dark conditions for 24 h to give $NQC_{15}S$-AuNP@PSI (Fig. 15C).

Reconstitution of PSI with $NQC_{15}S$-AuNP was identified by the activity test and TEM observation. The activity test by actinic blue-light irradiation to the intact PSI induced an absorption decrease at 701 nm by the formation of $P700^+$. This phenomenon was brought about by the higher rate of light-induced electron efflux from PSI in comparison with the rate of electron influx

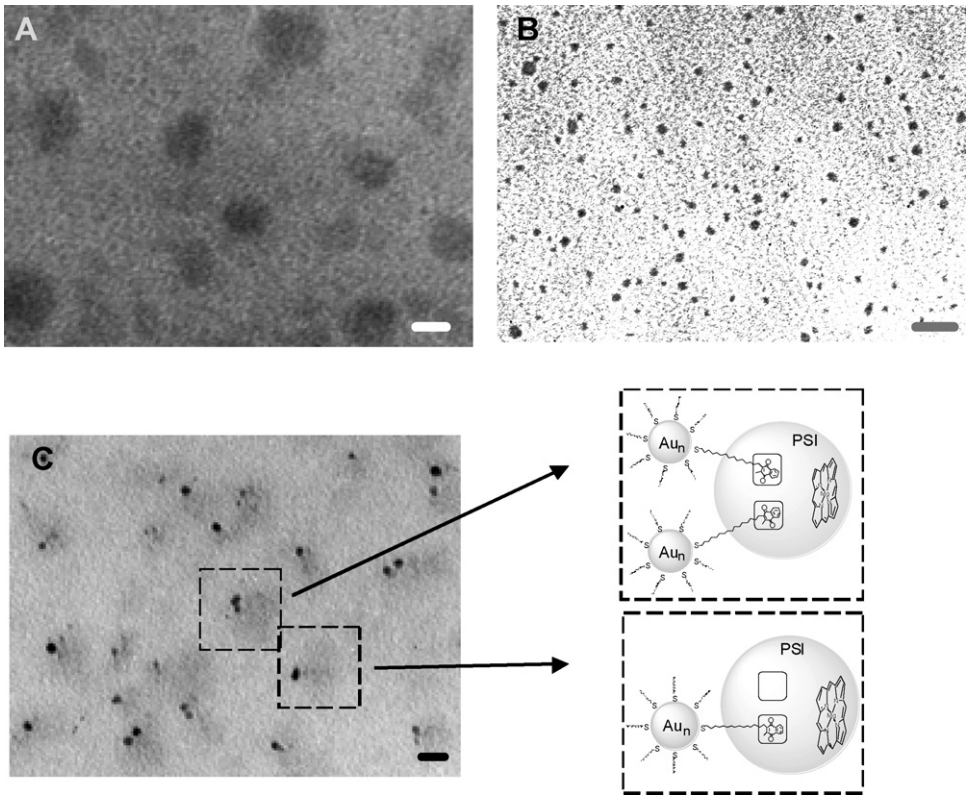


Fig. 16. TEM images of intact PSI (A), $NQC_{15}S$-AuNP (B), and $NQC_{15}S$-AuNP@PSI (C). The scale bar on each image is 10 nm. (reprinted with permission from Ref. [9]).

from NaAs to $P700^+$. The $VK_1$-free PSI showed little absorption change because of the quick backward electron transfer from $A_0$ to $P700^+$. The reconstituted PSI with $NQC_{15}$S-AuNP again showed a normal absorption decrease by blue-light irradiation. This indicated that the 2-methyl-1,4-naphthoquinone moiety of $NQC_{15}$S-AuNP fitted to the quinone pocket of PSI and worked as a mediator of the electron transport system in PSI.

A TEM image of the intact PSI shown in Fig. 16A exhibited gray circles with diameters of *ca.* 20 nm and *ca.* 10 nm. These sizes were assigned as a trimer (22 nm-o.d.) and a monomer (10 nm-o.d.) of PSI, respectively [78,79]. The TEM image of $NQC_{15}$S-AuNP in Fig. 16B appeared as black dots $1.6 \pm 0.5$ nm in diameter. In the image of $NQC_{15}$S-AuNP@PSI in Fig. 16C, both a large gray circle (10 nm-o.d.) and a small, clear, black dot (2 nm-o.d.) can be seen, and every gray circle (PSI) has one or two black dots ($NQC_{15}$S-AuNP). This stoichiometry indicates that there were no random aggregations and only connections via reconstitution at the $VK_1$ sites, because PSI has two $VK_1$ pockets.

Photocurrent action spectra of $NQC_{15}$S-AuNP@PSI chemically connected to a 1,4-benzenedimethanethiol SAM-modified gold electrode in the presence of sodium L-ascorbate (NaAs) as a sacrificial reagent and 2,6-dichloroindophenol sodium hydrate (DCIP) as a mediator in an MES–NaOH (pH 6.4) buffer solution containing $NaClO_4$ as an electrolyte at 0 V versus Ag/AgCl showed a clear peak at 680 nm, which is consistent with the absorption spectrum of PSI, indicating that these photocurrent responses were due to the photo-excitation of PSI.

Practical application of this system as an electronic imaging device was demonstrated by adapting the $NQC_{15}$S-AuNP@PSI to a gate of an FET (Fig. 17A). The reconstituted PSI was immobilized on a $Si_3N_4$–$Ta_2O_5$ thin layer on the gate of an FET using silane coupling reaction and Au–S bond formation. Thus, SAM was prepared on the gate of an FET in an ethanol solution of 5% bis[3-(triethoxysilyl)propyl] tetrasulfide for 1 h at room temperature, followed by the immersion of the FET gate in a buffer solution of $NQC_{15}$S-AuNP@PSI for 24 h. In the voltage–current characteristics of the $NQC_{15}$S-AuNP@PSI-modified FET, light irradiation at 670 nm induced a marked change in the voltage between the gate and the source ($V_{GS}$) from −3.3 V to −5.4 V when the current between the drain and the source ($I_{DS}$) was below 1 μA. The light intensity affected the magnitude of $V_{GS}$ (Fig. 17B), thus indicating the potential use of this system in the interpretation of a grayscale image.

In conclusion, we have fabricated a bio-photosensor made of cyanobacterial PSI coupled with a transistor via molecular wire. This system was able to sustain its original level of performance for a period of more than 1 year.

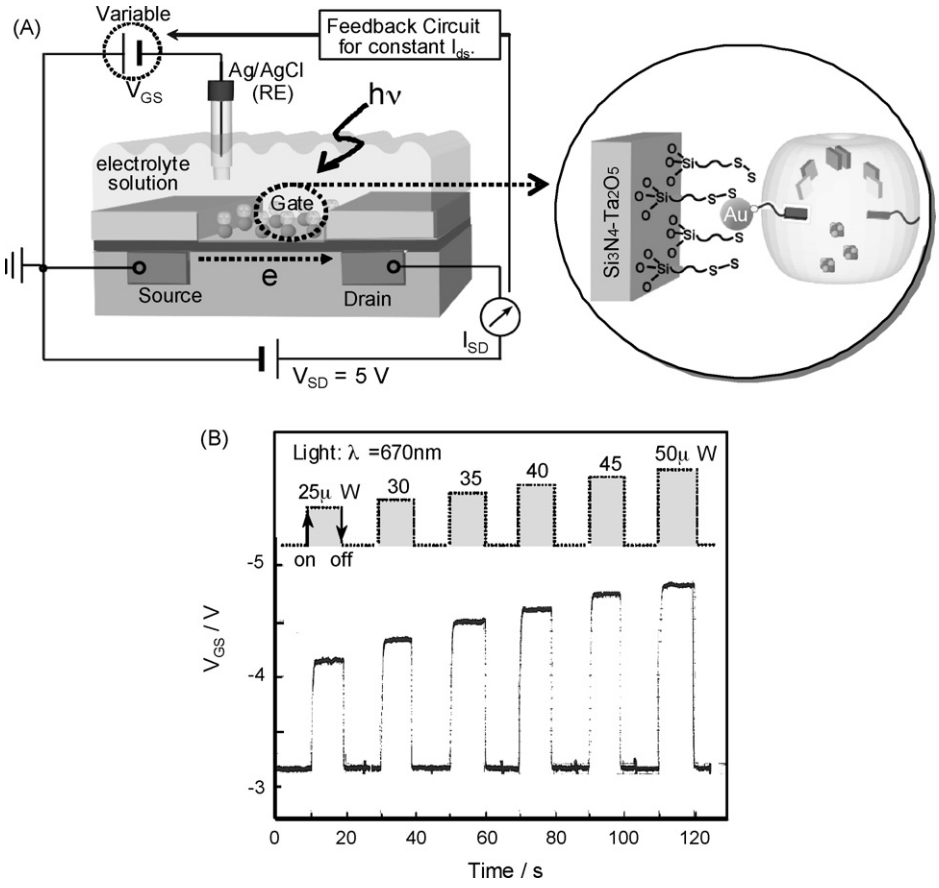


Fig. 17. Schematic illustration of the immobilization procedure of $NQC_{15}$S-AuNP@PSI on a field-effect transistor (FET) (A), and photo-response and light power dependency of $V_{GS}$ for the $NQC_{15}$S-AuNP@PSI immobilized FET in an MES–NaOH (pH 6.4) buffer solution containing 250 mM NaAs, 2.5 mM DCIP, and 100 mM $NaClO_4$. (B) (reprinted with permission from Ref. [9]).

## 4. Conclusion

In this article, we have discussed two issues in the construction of molecular wires and their electron transport behavior. The first topic involves a new fabrication method of hetero-structured molecular wires using surface coordination reactions. The molecular wires show intra-wire electron transport behaviors, which are essential characteristics for the fabrication of molecular devices. One advantage of this methodology is the possibility of introducing electro- and/or photo-functional chemical structures at desired positions in the wire in this method. The second topic shows a bottom-up method to fabricate a photo-sensor by combining a photo-responsive bio-molecule, molecular wire, and a gold nanoparticle on the transistor gate. Using PSI's molecular recognition ability, its connection with a molecular wire was successfully accomplished, leading to the stable photoresponse of the bio-photosensor. The final goal of this system is to sense a small number of photons by utilizing the single-electron transferability of a gold nanoparticle. Both topics demonstrate that the surface bottom-up fabrication of molecular wires is a useful approach to the development of molecular devices.

## Acknowledgements

The authors thank the following people who worked on the present study. Co-workers at the University of Tokyo are Dr. Tetsu Yonezawa, Dr. Shoko Kume, Dr. Masaki Murata, Dr. Katsuya Mizuno, and Yoshiki Ohba. Collaborators are Dr. Takashi Hiraga, Dr. Nao Terasaki, Dr. Noritaka Yamamoto, Dr. Kaoru Tamada, and Dr. Mineyuki Hattori at the National Institute of Advanced Industrial Science and Technology; Prof. Yasunori Inoue, Dr. Akihiko Tohri, Ikutaro Sato, Dr. Masako Iwai, Michinao Iwai, Shunpei Taguchi, and Prof. Isao Enami at Tokyo University of Science; Prof. Makoto Minakata and Dr. Satoshi Yoneyama at Shizuoka University; and Prof. Masaaki Fujii, Dr. Tsutomu Ohmori, and Dr. Makoto Sakai at Tokyo Institute of Technology. This work was supported partly by Grants-in-Aid from the Ministry of Education, Culture, Sports and Science of Japan, Grants-in-Aid for Special Coordination Funds for Promoting Science and Technology Leading Research, and The 21st Century COE Program for Frontiers in Fundamental Chemistry.

## References

[1] C. Joachim, J.K. Gimzewski, A. Aviram, Nature 408 (2000) 541.
[2] J. Park, A.N. Pasupathy, J.I. Goldsmith, C. Chang, Y. Yaish, J.R. Petta, M. Rinkoski, J.P. Sethna, H.D. Abruña, P.L. McEuen, D.C. Ralph, Nature 417 (2002) 722.
[3] C.E.D. Chidsey, R.W. Murray, Science 231 (1986) 25.
[4] M.S. Wrighton, Science 231 (1986) 32.
[5] H.B. Gray, J.R. Winkler, Proc. Natl. Acad. Sci. U.S.A. 102 (2005) 3534.
[6] K. Kanaizuka, M. Murata, Y. Nishimori, I. Mori, K. Nishio, H. Masuda, H. Nishihara, Chem. Lett. 34 (2005) 534.
[7] Y. Ohba, K. Kanaizuka, M. Murata, H. Nishihara, Macromol. Symp. 235 (2006) 31.
[8] Y. Nishimori, K. Kanaizuka, M. Murata, H. Nishihara, Chem. Asian J. 2 (2007) 367.
[9] N. Terasaki, N. Yamamoto, K. Tamada, M. Hattori, T. Hiraga, A. Tohri, I. Sato, M. Iwai, M. Iwai, S. Taguchi, I. Enami, Y. Inoue, Y. Yamanoi, T. Yonezawa, K. Mizuno, M. Murata, H. Nishihara, S. Yoneyama, M. Minakata, T. Ohmori, M. Sakai, M. Fujii, Biochim. Biophys. Acta, Bioenerg, in press.
[10] P.G. Pickup, R.W. Murray, J. Am. Chem. Soc. 105 (1983) 4510.
[11] P.G. Pickup, W. Kutner, C.R. Leidner, R.W. Murray, J. Am. Chem. Soc. 106 (1984) 1991.
[12] E.D. Chidsey, R.W. Murray, J. Phys. Chem. 90 (1986) 1479.
[13] J. Hjelm, R.W. Handel, A. Hagfeldt, E.C. Constable, C.E. Housecraft, R.J. Forster, Inorg. Chem. 44 (2005) 1073.
[14] G. Zotti, G. Schiavon, S. Zecchin, A. Berlin, G. Pagani, A. Canavesi, Synth. Met. 76 (1996) 255.
[15] R.W. Murray, Ann. Rev. Mater. Sci. 14 (1984) 145.
[16] H. Nishihara, K. Aramaki, J. Chem. Soc., Chem. Commun. (1985) 709.
[17] H. Nishihara, K. Aramaki, Chem. Lett. (1986) 1063.
[18] H. Nishihara, M. Noguchi, K. Aramaki, Inorg. Chem. 26 (1987) 2862.
[19] K. Sakamoto, H. Nishihara, K. Aramaki, J. Chem. Soc., Dalton Trans. (1992) 1877.
[20] P.G. Pickup, R.W. Murray, J. Electrochem. Soc. 131 (1984) 833.
[21] H.C. Hurrell, H.D. Abruña, Inorg. Chem. 29 (1990) 736.
[22] J. Ochmanska, P.G. Pickup, J. Electroanal. Chem. 297 (1991) 197.
[23] S.S. Zhu, T.M. Swager, J. Am. Chem. Soc. 119 (1997) 12568.
[24] H.J. Dahms, Phys. Chem. 72 (1968) 362.
[25] I. Ruff, V.J. Friedrich, J. Phys. Chem. 76 (1972) 162.
[26] D.N. Blauch, J.-M. Savéant, J. Am. Chem. Soc. 114 (1992) 3323.
[27] M. Abe, T. Michi, A. Sato, T. Kondo, W. Zhou, S. Ye, K. Uosaki, Y. Sasaki, Angew. Chem. Int. Ed. 42 (2003) 2912.
[28] M. Maskus, H.D. Abruña, Langmuir 12 (1996) 4455.
[29] M. Haga, T. Takasugi, A. Tomie, M. Ishizuya, Y. Yamada, M.D. Hossain, M. Inoue, Dalton Trans. (2003) 2069.
[30] M. Wanunu, A. Vaskevich, A. Shanzer, I. Rubinstein, J. Am. Chem. Soc. 128 (2006) 8341.
[31] G.F. Swiegers, T.J. Malefetse, Chem. Rev. 100 (2000) 3483.
[32] S. Leininger, B. Olenyuk, P.J. Stang, Chem. Rev. 100 (2000) 853.
[33] A.B. Descalzo, R. Martínez-Máñez, F. Sancenón, K. Hoffmann, K. Rurack, Angew. Chem. Int. Ed. 45 (2006) 5924.
[34] M. Altman, A.D. Shukla, T. Zubkov, G. Evmenenko, P. Dutta, M.E. van der Boom, J. Am. Chem. Soc. 128 (2006) 7374.
[35] L. Kosbar, C. Srinivasan, A. Afzali, T. Graham, M. Copel, L. Krusin-Elbaum, Langmuir 22 (2006) 7631.
[36] C. Lin, C.R. Kagan, J. Am. Chem. Soc. 125 (2003) 336.
[37] A.R. Guadalupe, D.A. Usifer, K.T. Potts, H.C. Hurrell, A.-E. Mogstad, H.D. Abruña, J. Am. Chem. Soc. 110 (1988) 3462.
[38] P. Daum, J.R. Lenhard, D. Rolison, R.W. Murray, J. Am. Chem. Soc. 102 (1980) 4649.
[39] K.-N. Kuo, R.W. Murray, J. Electroanal. Chem. 131 (1982) 37.
[40] P. Burgmayer, R.W. Murray, J. Electroanal. Chem. 135 (1982) 335.
[41] S. Nakahama, R.W. Murray, J. Electroanal. Chem. 158 (1983) 303.
[42] K. Sigehara, N. Oyama, F.C. Anson, J. Am. Chem. Soc. 103 (1981) 2552.
[43] C.R. Martin, I. Rubinstein, A.J. Bard, J. Am. Chem. Soc. 104 (1982) 4817.
[44] H.S. White, J. Leddy, A.J. Bard, J. Am. Chem. Soc. 104 (1982) 4811.
[45] L. Roullier, E. Waldner, E. Laviron, J. Electroanal. Chem. 139 (1982) 199.
[46] L. Roullier, E. Waldner, J. Electroanal. Chem. 187 (1985) 97.
[47] J.G. Eaves, H.S. Munro, D. Parker, Inorg. Chem. 26 (1987) 644.
[48] R.A. Saraceno, G.H. Riding, H.R. Allcock, A.G. Ewing, J. Am. Chem. Soc. 110 (1988) 7254.
[49] R.P. Buck, J. Phys. Chem. 92 (1988) 4196.
[50] J.-M. Savéant, J. Electroanal. Chem. 242 (1988) 1.
[51] J.-M. Savéant, J. Phys. Chem. 92 (1988) 1011.
[52] J.-M. Savéant, J. Phys. Chem. 92 (1988) 4526.
[53] A.J. Bard, L.R. Faulkner, Electrochemical Methods: Fundamentals and Applications, 2nd ed., Wiley, New York, 2001.
[54] D. Chen, G. Wang, J. Li, J. Phys. Chem. C 111 (2007) 2351.
[55] K. Kinbara, T. Aida, Chem. Rev. 105 (2005) 1377.
[56] E. Katz, I. Willner, Angew. Chem. Int. Ed. 43 (2004) 6042.
[57] C.M. Niemeyer, Angew. Chem. Int. Ed. 40 (2001) 4128.

[58] Y. Xiao, F. Patolsky, E. Katz, J.F. Hainfeld, I. Willner, Science 299 (2003) 1877.
[59] O. Lioubashevski, V.I. Chegel, F. Patolsky, E. Katz, I. Willner, J. Am. Chem. Soc. 126 (2004) 7133.
[60] R. Emerson, R.V. Chalmers, C. Cederstand, Proc. Natl. Acad. Sci. U.S.A. 43 (1957) 133.
[61] R. Emerson, R.V. Chalmers, C. Cederstand, M. Brody, Science 123 (1956) 673.
[62] A.F. Janzen, M. Seibert, Nature 286 (1980) 584.
[63] R. Bhardwaj, R.L. Pan, E.L. Gross, Nature 289 (1981) 396.
[64] I. Lee, J.W. Lee, E. Greenbaum, Phys. Rev. Lett. 79 (1997) 3294.
[65] E. Katz, J. Electroanal. Chem. 365 (1994) 157.
[66] B.S. Ko, B. Babcock, G.K. Jennings, S.G. Tilden, R.R. Peterson, D. Cliffel, E. Greenbaum, Langmuir 20 (2004) 4033.
[67] T. Yamaoka, K. Satoh, S. Satoh, Plant Cell Physiol. 19 (1978) 943.
[68] H. Koike, K. Satoh, S. Katoh, Plant Cell Physiol. 23 (1982) 293.
[69] B.L. Epel, J. Neumann, Biochim. Biophys. Acta 325 (1973) 520.
[70] M. Iwaki, S. Ito, FEBS Lett. 256 (1989) 11.
[71] P. Jordan, P. Fromme, H.T. Witt, O. Klukas, W. Saenger, N. Krauβ, Nature 411 (2001) 909.
[72] P. Fromme, P. Jordan, N. Krauβ, Biochim. Biophys. Acta 1507 (2001) 5.
[73] K. Brettel, Biochim. Biophys. Acta 1318 (1997) 322.
[74] S. Bahatyrova, R.N. Frese, C.A. Siebert, J.D. Olsen, K.O. van der Werf, R. van Grondelle, R.A. Niederman, P.A. Bullough, C. Otto, C.N. Hunter, Nature 430 (2004) 1058.
[75] A. Ben-Shem, F. Frolow, N. Nelson, Nature 426 (2003) 630.
[76] C.W. Mullineaux, M.J. Tobin, G.R. Jones, Nature 390 (1997) 421.
[77] S. Chen, R.S. Ingram, M.J. Hostetler, J.J. Pietron, R.W. Murray, T.G. Schaaff, J.T. Khoury, M.M. Alvarez, R.L. Whetten, Science 280 (1998) 2098.
[78] S.-O. Wenk, J. Kruip, J. Chromatogr. B 737 (2000) 131.
[79] T.S. Bibby, J. Nield, J. Barber, Nature 412 (2001) 743.